CONF-9006153--3
UCRL- 102304
PREPRINT

INTERACTIVE SHOCK STRUCTURE RESPONSE TO PASSAGE THROUGH TURBULENCE

Alfred C. Buckingham

This paper was prepared as an American Institute of Aeronautics and Astronautics archival paper, AIAA 90-1642, for presentation at the AIAA 21st Fluid Dynamics, Plasma Dynamics and Lasers Conference, Seattle WA, June 18-20, 1990, and for submittal to the AIAA Journal.

June 6, 1990

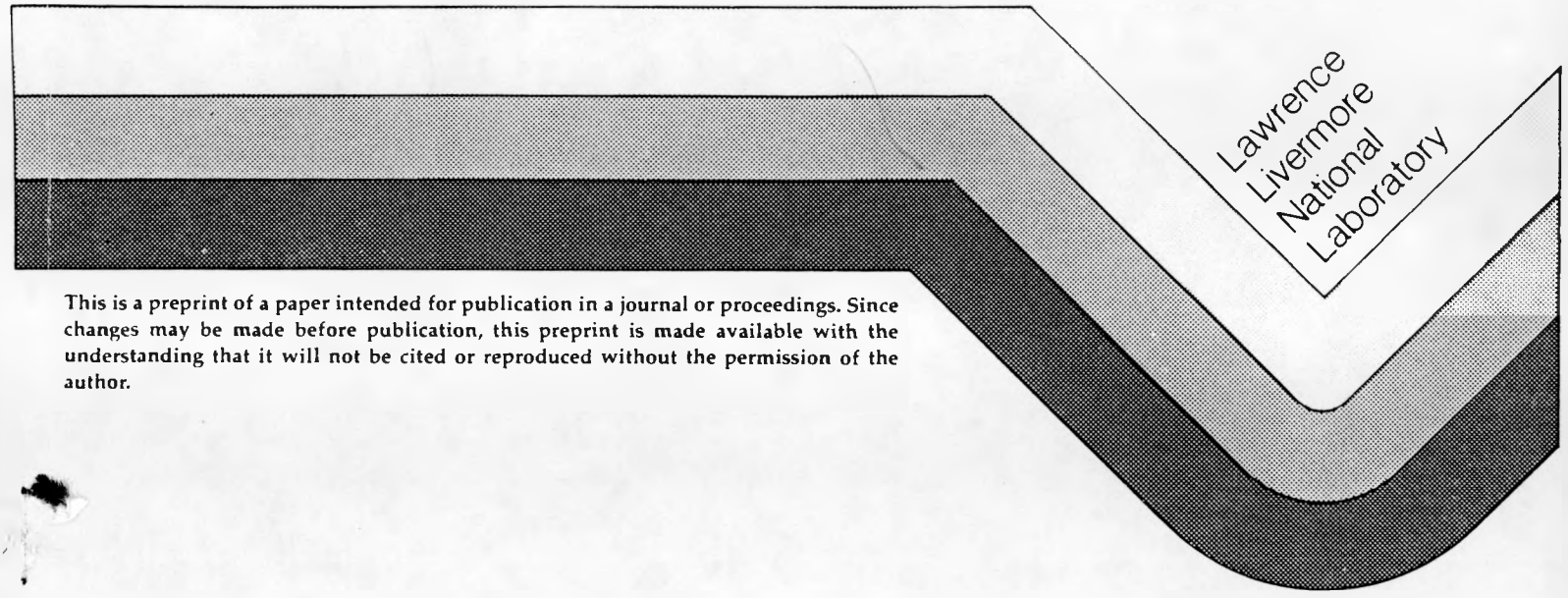

INTERACTIVE SHOCK STRUCTURE RESPONSE TO PASSAGE THROUGH TURBULENCE*

Alfred C. Buckingham†

Center for Compressible Turbulence
University of California, Lawrence Livermore National Laboratory
Livermore, California 94550

UCRL--102304

DE90 013293

Abstract

This discussion is on the apparent random changes to shock transitional velocity, density, and temperature induced when weak- to moderate-strength shocks interact with relatively intense, preshocked turbulence. The shock fronts appear to ripple or distort randomly and unsteadily. Shocks amplify and alter the spectral structure of turbulent fields with which they interact. Questions develop about the mechanisms significant in this interaction. Consideration is given to the significance of this process in enhancing turbulent mixing and transport, and to the evolution and decay of the intensified turbulence during and after such an interaction process. Analysis of this process should provide insight and a firmer basis for the development and test of more effective, consistent compressible turbulence models, and for the interpretation, design, and analysis of related experiments. At the present stage, particular emphasis is placed on determining estimates of the gross partition of directed shock energy into turbulent kinetic energy, and on fine-scale modal partition between acoustic, entropy, and vorticity fields during interactions.

Introduction

In this work, stochastic numerical simulations are used to examine shockwave interaction regions that are too small and time intervals too brief to permit adequate experimental access and resolution. The simulations trace the evolution of structure (velocity, temperature, density profiles) within a spatially and temporally distorted shock front. Shock distortions develop as the shock front advances through and interacts with upstream turbulence.

Conceptually, shockwave interactions couple directed shockwave translational energy into turbulence kinetic energy during shock transition. The intensity of the turbulence is amplified and its spectra altered. The changes to the turbulence and shockwave structure is most apparent when relatively low Mach Number shockwaves encounter strong turbulence. However, some evidence and considerable theoretical speculation suggests that significant shock enhancement of turbulence may be evident at higher Mach Numbers.

* This is a report of work performed under the auspices of the U.S. Department of Energy by the Lawrence Livermore National Laboratory under Contract No. W-7405-Eng-48.

†Physicist, Fluidynamics, Associate Fellow, AIAA.

Turbulence amplification by shock-waves is illustrated by some experimental shockwave-boundary layer and shock tube intensity amplification results shown in Fig. 1. These experimental results at low Mach Number are supplemented at somewhat higher Mach Numbers by some results from small perturbation linear theory[1] and some more recent theoretical analyses and computations.[2,3,4,5] The figure illustrates the amplification of the initial rms turbulence velocity when the turbulence is encountered by a plane shock moving into the turbulent field. Amplification may increase somewhat with shock Mach Number although linear theory suggests the amplification may increase at a lesser rate up to Mach Numbers of about 10.

Recently, minimally diffusive, high resolution Godunov method shockwave computations have been applied to examine the effects of this interaction amplification process on prescribed initial turbulence.[4] Figure 2 shows a numerical simulation of a Mach 2.3 shock wave advancing through initially prescribed turbulence. Note that the computed shock front develops spatial distortions under the influence of the random turbulent vortical field into which it moves. The numerics can only simulate qualitative behavior; however, characteristically similar deformations of the shock surface have been seen in low Mach Number, high turbulent intensity interaction experiments, cited in recent studies.[3,4] The experimental observations suggest that at low Mach Numbers, the weaker shock waves deform, ripple and, perhaps, break up into shocklets during encounters with intense turbulence. In these situations, the shock influence on amplifying the turbulence and redistributing the random flow structure is quite modest, although by no means negligible. At higher shock Mach Numbers the amplification and alteration to the pre-shocked turbulence is much more pronounced although the changes to the shock wave itself are much less evident.

Almost 80 years ago, Taylor[6] illustrated that, to leading order, the shock-front thickness depends directly on the gas phase molecular transport properties and inversely on the shock strength and gas density. In the present analysis, it is anticipated that statistical realizations may be developed which display analogous influences from turbulent eddy dynamical thickening and distortion in the neighborhood of the shock front.

Resolving the partition of energy, between the directed shock energy and the turbulent kinetic energy requires information from higher-than-leading- order interaction considerations. Strong coupling must be properly accounted for between all three modes: acoustic,

entropy, and vorticity. This is particularly evident at the shock front where the nonlinear steepening of the wave modes suggests the attention that must be placed on scale coalescence during interaction and immediately following shock passage. Kovasznay's[7] seminal analysis of almost 35 years ago implies that strong, interactive coupling first emerges at the third order in terms of the asymptotic structure of the modal interaction. Analysis and stochastic simulations of the turbulence-altered shock transition distributions[12] and development and test of a mesh-grid scale viscoelastic shock interaction response model on continuously remapped arbitrary Lagrange-Euler mesh code[11] are among the topics discussed here.

Discussion

Monte-Carlo Shock Interaction

At this point it is useful to provide a discussion of the random choice procedure used to obtain both realizations and ensemble averages of the transition distributions through turbulence-distorted shock fronts. The basic idea is to combine the distributions of fluctuating velocity, temperature and density from two reservoirs. One is ahead of and the other behind the shock in an instantaneous realization. In principle, the technique, although not the procedure, follows the Mott-Smith[8] theoretical outline and the Bird[9] Monte-Carlo numerical procedure for analysis of shock structure on a molecular kinetic theory basis. However, the substantial difference in the interaction scale sizes, longer relaxation times and inherent rotationality, require a fundamental change in the basic procedure and the spatial dimensions (at least two-dimensional fields must be considered). The interactive random sampling must take place over a much larger extent of *continuous* transitional probability distribution space.[12]

Consider a turbulence-distorted segment of a plane normal shockwave propagating at a mean speed, $\bar{U}_s$, in the two- dimensional domain, $\tilde{\alpha}$ (ξ, η), illustrated in Fig. 3. The oscillating, distorted shock front surface shown as the sinuous solid line, conceptually sweeps out an average projected distance, $\Delta\bar{\xi} = \delta_s(\xi, t, t + \Delta t)$, in some discrete increment of time, Δt, sufficiently small to resolve the several scales of irregular motion selected to represent the influence of shock interaction with a turbulent field. Average shock displacement and ensemble averages are formed from individual realizations taken through the shock interaction region along selected horizontal slices, η_i, as indicated in Fig. 3.

A comprehensive discussion of the stochastic approximation applied to random perturbations of the transition variables, subject to discontinuous mean stationary (Hugoniot) and unsteady (acceleration of front) conditions, is provided in a previous description.[12] Here, in the interest of conserving space, we will confine the discussion to an outline of the essential features, assumptions and convergence tests for the adequacy of the sampling intervals and population.

In parallel with the Mott-Smith[8] formal expansion procedure for interactions of bivariant statistical populations of velocity distribution on a molecular level, on a continuum flow, perturbation level, the present concept is based on the modeled interaction of two randomly distributed populations of velocity, u', internal energy, e', and density, ρ'. One distribution, $D^{(1)}$, is ahead of the shock, the other, $D^{(2)}$, is behind the unsteadily distorted, advancing shock front. Each distribution is represented by several hundred particles which interact at about 10 discrete positions, , N = 1,9 over the range R(O, δ_s) along a slice, η_i. For kinetic theory shock structure computations, Bird[9] has developed numerical procedures which provide convergent one-dimensional statistical distributions of the molecular velocity field in plane shock transition with as few as 10,000 collisional interactions at 10 discrete intervals over a shock thickness. In our application, the field of interaction of the continuum (but statistically perturbed flow) is a dimension, δ_s, thousands to tens of thousands of molecular shock thickness. Nonetheless, convergence as determined by a smooth distribution of the velocities in the equilibrium sense has been achieved by less than equal to 10,000 individual statistical encounters for each of the three transitional variables. Numerical encounters until the preselected equilibrium smoothness criterion is met. Monte Carlo importance sampling procedures have been used to speed convergence.[12]

Redistribution of the variables at the shock front provides a statistical population of mass, Eqn. (1), momentum, Eqn. (2), and energy, Eqn. (3), which together meet both mean (Hugoniot) and acceleration constraints in nonstationary planar shock transition systems.

$$D_\xi \left[\begin{array}{c} dM(\xi) = \rho_{(0)}\phi'_{(0)} - \rho_{(1)}\phi'_{(1)} \\ dM(\xi) = \left(\rho_{(0)}U'_{(0)}\right)\phi'_0 - \left(\rho_{(1)}U'_{(1)}\right)\phi'_1 - \left(p'_{(0)} - p'_{(1)}\right) \\ dM(\xi) = \rho_{(0)}q^2_{(0)}\phi'_{(0)} - \rho_{(1)}q^2_{(1)}\phi'_{(1)} + 2\left(\rho_{(0)}e_{(0)}\phi'_0 - \rho_{(1)}e_{(1)}\phi'_1\right) \\ + 2\left(p_{(0)}u'_{(0)} - p_{(1)}u'_{(1)}\right) \end{array} \right] \quad (1\text{-}3)$$

In addition to the parallel velocity fluctuating component, u, the density, ρ, and the internal energy, e, we have introduced the fluctuating pressure, p' and the notation (0), (1) to represent pre-shocked and post-shocked variable statistical distributions and the total velocity

$$q^2_{(1)} \equiv u^2_{(1)} + v^2_{(1)}\,, \quad q_{(1)} = (q_{(1)}) + q'_{(1)} \tag{4}$$

and relative fluctuational velocity with respect to the instantaneous mean shock velocity,

$$\phi'_{(1)} \equiv \left(u'_{(1)} - \bar{U}_s(\eta_i)\right)\,. \tag{5}$$

The one-dimensional, η level, statistical distributions provide sharp transitions and pre- and post-shock statistical interaction populations of the perturbational velocity, density, and energy. This is illustrated by the computed single η level realizations of streamwise velocity, u, at mean shock Mach Numbers of 6, 3, and 2. This may be reviewed in Fig. 4. The contraction of the shock distortion interaction regions as the Mach Number increases is also clearly evident in this figure.

The single-level statistical results taken at many discrete levels, η, provide the basis for approximating the perturbationally accelerated and deformed shock front and turbulence quantities through transition.

A full two-dimensional combination of these influences is approximated for the deforming shock front for which both mean and perturbational boundary conditions must be applied as well as the influence of both streamwise and tangential mean and perturbational components. The constitutive relations for the perturbational field and the thermodynamic state of the pre- and post-shocked regions are undetermined, hence, the system is ill-posed in the absence of a careful definition of the shock transition process and its boundary conditions in a turbulent field. This can be best appreciated by reviewing, for example, Emanuel and Liu's persuasive description of the properly defined state and dynamic conditions for stationary and accelerating shockwaves of arbitrary shape.[10]

Here we approximate the distorted shock front by continuous functional shape factors, $\Lambda\,(\xi,\eta)$ which are necessarily continuous and analytic through second order, consistent with the shock curvature and local entropy production interdependence.

Local kinematics demand that

$$\bar{U}_s(\eta_i) = \frac{\hat{n}}{|\nabla\Lambda|}\,\frac{\partial\Lambda(\eta_i)}{\partial t}$$

$$\text{and}\quad \frac{D\Lambda(\eta_i)}{\partial t}\,\Big|_s = \frac{\partial\Lambda(\eta_i)}{\partial t} + \bar{U}_s(\eta_i)\cdot\nabla\Lambda = 0\,, \tag{6}$$

where $\hat{n}(\xi,\eta)$ is a local unit normal vector with respect to the perturbed shock front.

We combine the previous Pdf realizations, the boundary conditions and the evolution of the shock profile by forming instantaneous tendency equations in the two-dimensional plane. Derivatives and the geometrical influences of the distorted shock surface are approximated in phase space using fast fourier transforms on a spectral expansion from 0 to 2π over the selected range η_o to η_{final} of discrete, equally spaced shock transition slices, Fig. 3.

At this second stage, instantaneous two-dimensional (ξ,η) relations are formed to evaluate $q(\Lambda',\Lambda'')$. Define a functional $\Lambda = f(\eta)$, continuous and analytic through Λ' and Λ''. This permits continuous evaluation of the evolution of the shock shape, slope, and curvature, κ,

$$\kappa(\Lambda) \equiv \Lambda'' \equiv \frac{d\Lambda'}{dS_\Lambda} = \frac{f_{,\eta\eta}}{\left[1 + (f_{,\eta})^2\right]^{3/2}} \tag{7}$$

while u,v may be evaluated consistent with the local vorticity/curvature theorem. The η derivatives are formed by transforming $F(\eta) = \rho,e,u,v,\Lambda,\Lambda',\Lambda''$ over $\eta c[o,2\pi]$,

$$F(\eta) = \sum_{k=-k}^{k^*} F_k \exp(1k\eta) \tag{8}$$

The tendency equations are then formed over the two-dimensional shock-turbulence interaction region, $\Lambda(\xi,\eta)$,

$$\{A\}_{,t} = \{B\}_{,I} \qquad I = \xi,\eta$$

$$\{A\} \equiv \begin{Bmatrix} \rho \\ \rho U^l \\ \rho_e \end{Bmatrix} \qquad \{B\} \equiv \begin{Bmatrix} \rho U^l \\ \rho U^l U^j + p \\ \rho e^j + \rho U^j \end{Bmatrix} \tag{9}$$

In the third stage, we integrate the tendency equations from t_o to $t_o + \Delta t$. We use an explicit, third order Runge-Kutta procedure, forming

$$\{A\}(t_o + \Delta t) = \int_{t_o}^{t_o+\Delta t} \{A\}_{,t}\, dt \rightarrow J(t_o + \Delta t) \tag{10}$$

Obtain effective distributions $D(U^l)$, $D(\rho)$, $D(e)$ for $(\xi = O, \delta_s, \forall\eta)$, satisfying J, the transitional stationary and accelerating jump conditions. We also obtain the effective shock thicknesses, δ_s, by satisfying J under the integral mass, momentum and energy conservation constraints.

In Table I, some of the results of the stochastic simulations are summarized for shock Mach Numbers, M=2, M=3, and M=6. In the second column, the shock turbulence interaction thickness, (δ_s) is normalized with respect to its value at M=2, showing a relative compression of the interaction region to about 75% of its M=2 value at M=3 and to about 25% of its M=2 value at M=6. One-dimensional spatial autocorrelations of the streamwise component, u, yield relative fluctuating integral scales of the interactions occupying nearly 33% of δ_s at M=2, but falling off to 5% and 2.4% at M=3 and M=6, respectively. The fourth column identifies the computationally simulated amplification of the streamwise fluctuating velocity component which has an average value of 3.2, 4.1, and 5.2 at simulated Mach Numbers of 2, 3, and 6, respectively.

M	Δ	$\frac{1}{X}\int Y_{xx}\,dX$	A_I
2.0	1.0	3.286E-01	3.20
3.0	0.7667	5.010E-02	4.10
6.0	0.2502	2.380E-02	5.20

Table I.

Ensemble Averages, Modal Partition

Probability density functional distributions of the rms fluctuational quantities are obtained as ensemble averages of the individual realizations at several level planes, η_i. Analysis of these results produces estimates of the modal energy partition between velocity (U), internal energy, (E, associated with the acoustic fluctuational field), and density (ρ, associated with the entropy fluctuational field).

In Fig. 5 we have plotted the foregoing Pdf's at three different levels of the interactive shock front propagating into a prescribed turbulence field at a shock Mach No. of 3. Also shown is a shadowgraph projection of the individual shock deformational movement over an interaction distance, δ_s, traversed in a total evolutionary time increment, Δt.

Similar results, over a significantly compressed dynamical interaction range, δ_s, are shown for a shock Mach Number of 6 in Fig. 6.

In Table II are summaries of the computer experiments on energy modal partition at Mach 2.0, 3.0, and 6.0. The modes are identified together with the percentage of the total fluctuational energy averaged over the entire interaction region, δ_s. The results indicate that there is almost an equal partition of energy shared by velocity (du) and entropy (ds) fluctuating fields. Surprisingly (to us) the acoustical fluctuational field share dp(c) is for less than that shared by the velocity and entropy. Considerable shock translational energy is distributed in the acoustic field, however, the results here only reflected the fluctuational components, not the mean or the low wave-number contributions. Our analysis of this surprising result continues. The last column essentially gives the ratio of the directed shockwave (diabatic) energy budget that is transferred to the "adiabatic" turbulent modes. It shows that substantially more difficulty exists at higher Mach Numbers in coupling shock energy to turbulence. However, the increase in shock energy available at higher Mach Numbers almost compensates.

Mach No.	% dU	% dS	% dp(c)	Adiab /Diab
2.0	53.0	45.0	2.0	14.0
3.0	50.0	47.5	2.5	1.8
6.0	48.8	48.0	3.2	0.3

Table II.

It is of interest to examine another aspect of shock oscillations and irregular shock deformations. The irreversible transfer in shock transition decreases for oscillating shocks in comparison to their stationary counterparts. On the debit side, corrections to experiments have to be made since the total pressure change is greater and the entropy less than for the stationary counterparts for which the total pressure instruments are calibrated. On the credit side, the shock induced drag deficit is reduced. This factor may have some impact on supersonic cruise aerodynamic configuration design or for supersonic combustion with unsteady shockwave-induced mixing at a lessened cost to inlet drag.

Some 15-year-old experiments in Japan on resonant tubes in low (M=2) supersonic flow help to bracket this oscillating shock influence.[13] It is of interest here to examine our current results with respect to this decreased entropy dynamic state for oscillating shocks. Figure 7 shows the nominal oscillating frequency of the shock field as a function of Mach Number from the present computations in comparison to the experimental values for resonant tubes.[13] Figure 8 shows a prediction of the lowered entropy in comparison to the non-oscillating shock with experimental resonance tube values superimposed. This effect appears to show promise for supersonic cruise aerodynamic drag reduction and lowered drag penalty for shock-enhanced supersonic combustion.

Viscoelastic Response

Some of our attention in the current studies emphasizes the need for better approaches to modeling or compensating for the subgrid range of scale motions which are unresolved in large-eddy simulations. In particular, for application to compressible, high-speed aerodynamics the compatibility between a subgrid model, closure and feedback to grid-scale motions is being studied. At present, experiments are being run using the model concept of the shock turbulence interaction as a viscoelastic response of two overlapping dynamic systems. Figure 9 shows some of our current numerical LES experiments using this concept for dynamically coupling shock influences on turbulence.

In these simulations, trial solutions with different response parameters are covered from computations on an arbitrary Lagrange-Euler compressible (ALE) code version with a choice of subgrid models.[11] Guidance on the viscoelastic metastable modulus level and temporal decay are developed from the Monte-Carlo shock dynamic simulations discussed here and shown as a trace response of the buildup of turbulence kinetic energy through the shock transition reigon in Fig. 9. Also shown are several best calculations using different, labeled pressure-buoyancy production and energy dissipation coupling models. A trace of the numerical dissipation, Q, shock damping term classically used for time-explicit Euler equation shock-capturing computations is also shown for three different grid resolutions. The present work indicates this is unnecessary in the presence of a properly matched shock/turbulence subgrid closure model.

Summary

The effects of Mach Number increase appear to favor a coalescence of interaction times and length scales between acoustic, entropy and vorticity modes. This convergence of scale sizes, however, probably does not persist indefinitely.

Our preliminary studies imply a divergence in scale sizes when the Mach Number increase reaches the hypersonic range.

The corresponding amplification rates increase less and less with increasing Mach Number and, perhaps, diminish at high Mach Numbers to distinct limiting values.

The persistence or duration of the shockwave-to-turbulence amplification influence seems to drop off with increasing Mach Number and increasing Reynolds Number.

A turbulent subgrid closure model may overcompensate for "Q" in shock damping, but it may be a closer representation of the natural situation if both dilatational and deformational components of shear are included in the shock-front-explicit damping term. Linear viscoelasticity appears consistent, appropriate and effective for modeling the interactive response in the transition region between advancing shock front and residual post-shock turbulent fields. We intend to pursue this further on both a theoretical and numerical trial basis with special attention to the subgrid resolution problem that develops when adapting a turbulence model for use on a finite mesh.

References

1. McKenzie, J.F. and Westphal, K.O.,*Physics of Fluids 11*, November 1968, pp. 2350-2362.

2. Zang, T.A., Hussaini, M.Y., and Bushnell, D.M., *AIAA J.* **22**, (1), 1984, pp. 13-21.

3. Buckingham, A.C., *Numerical Methods in Laminar and Turbulent Flow, v, Part 2*, ed. C. Taylor, Pineridge Press, Swansea, UK, 1987, pp. 963-974.

4. Buckingham, A. C., in *41st Annual Mtg, Div. of Fluidynamics, APS*, State University of New York, Buffalo NY, 1988.

5. Rotman, D., "Shock Wave Effects on a Turbulent Flow", MS undergoing revision for *Physics of Fluids*, 1989.

6. Taylor, G.I., *Proc. Royal Society London, A 84*, 1910, pp. 371-377.

7. Kovasznay, L.S.G., *J. Aero. Sci. 20*, October 1953, pp. 657-682.

8. Mott-Smith, H.M., *Phys. Rev. 82*, 1951, p. 885.

9. Bird, G.A., *J. Fluid Mech. 30*, 1967, pp. 479-487.

10. Emanuel, G., Liu, M.-S., *Phys. Fluids* **31**, (12), 1988, p. 3625.

11. Demuth, R.B., Margolin, L.G., Nichols, B.D., Adams, T.F., and Smith, B.W., *SHALE: A Computer Program for Solid Dynamics*, Los Alamos National Laboratory, Los Alamos NM, LA-10236, 1985. Also private communications with L.G. Margolin at Lawrence Livermore National Laboratory, 1988, 1989.

12. Buckingham, A.C., *Numerical Methods in Laminar and Turbulent Flow, VI, Part 1*, eds. C. Taylor, P. Gresho, R.L. Sani, J. Hauser, Pineridge Press, Swansea, UK, 1985, pp. 805-814.

13. Shigemi, M., Koyama, H., and Alhara, Y., "A Note on the Oscillating Shock Wave — Some Experiments", *Trans. Japan Soc. Aero. & Space Sciences* **19**, (44), 21976, pp. 68-81.

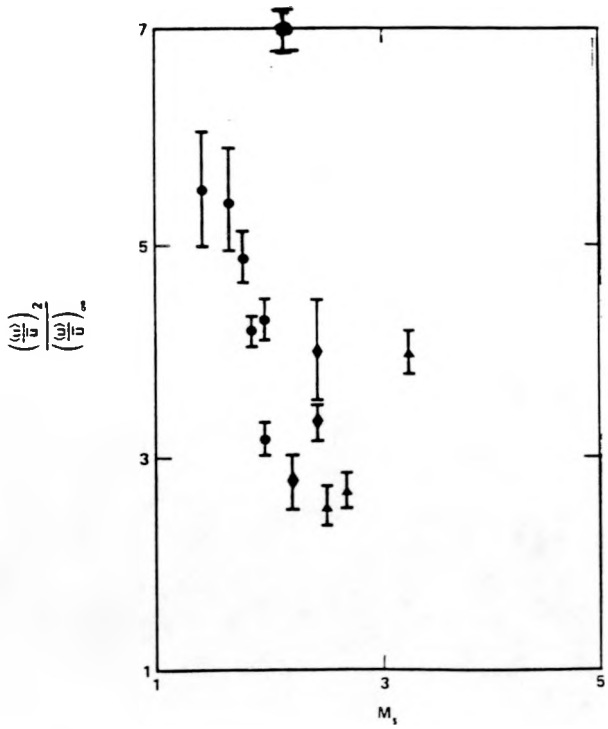

Fig. 1. Experimental amplification of streamwise component of perturbational velocity by interaction with a shock wave at specified Mach Number.

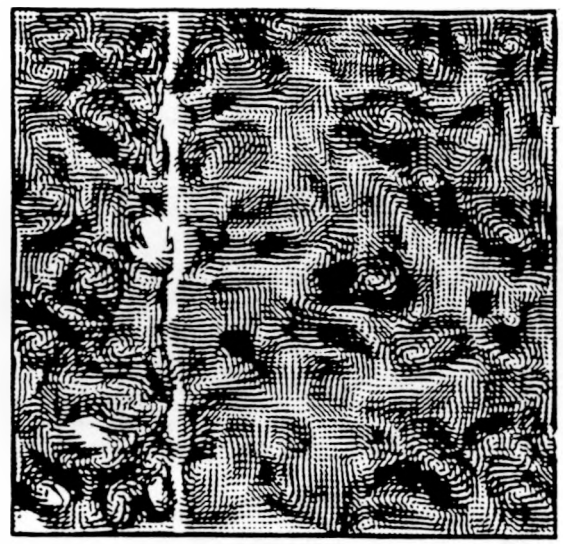

Velocity Field

Fig. 2. Computer simulations of a Mach 2.3 shock wave interacting with a randomly perturbed velocity field, Ref. 5.

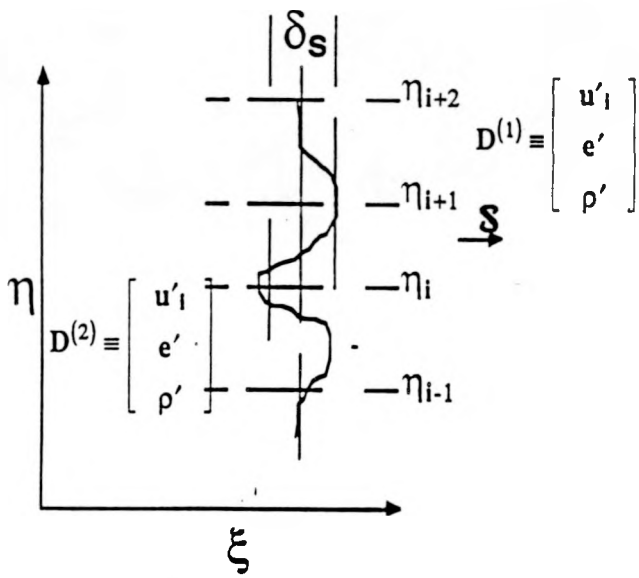

Fig. 3. Configuration space for discrete stochastic Monte-Carlo integral approximations of shock front structure changes during interaction with turbulence.

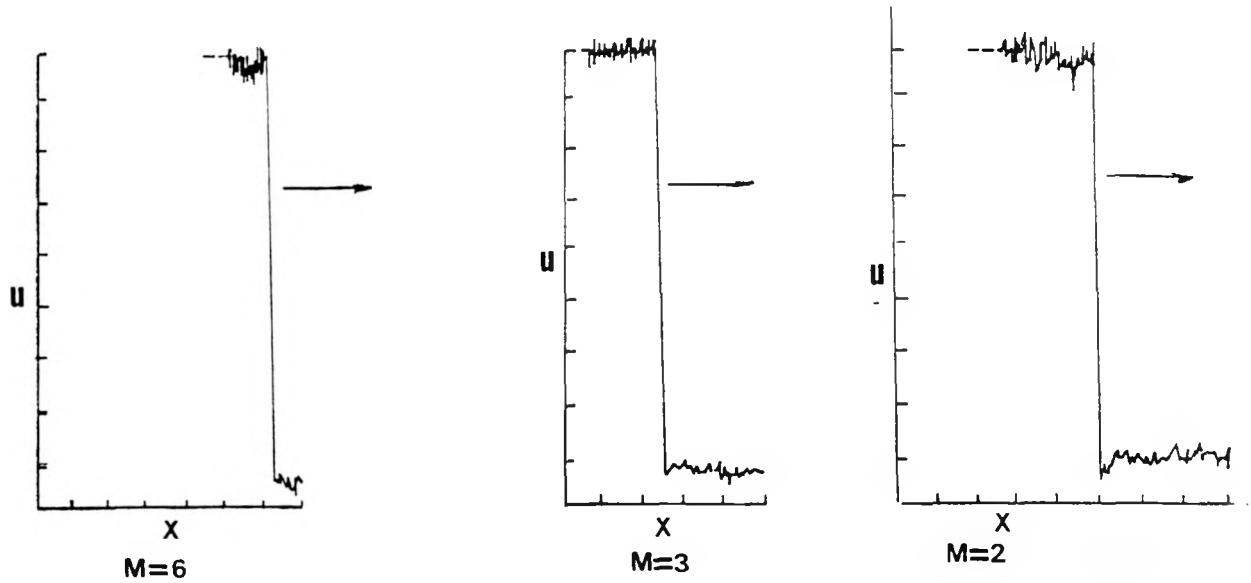

Fig. 4. Individual realizations of random velocities at discrete (η) levels from Monte-Carlo shock interaction simulations at M = 2, 3, and 6.

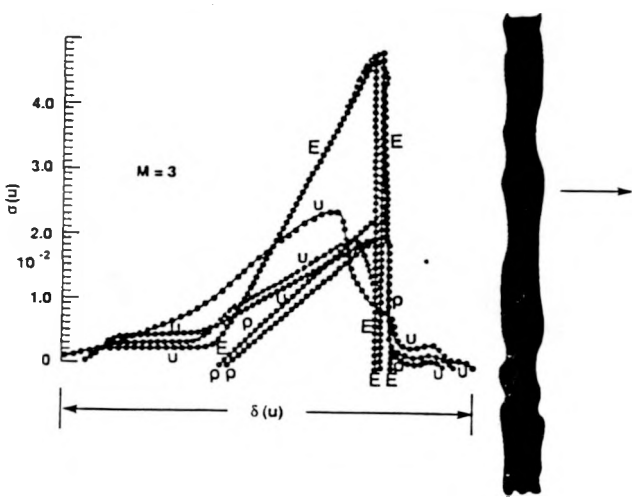

Fig. 5. Ensemble averaged pdf's of individual realizations for internal energy (E), velocity (U), and density (ρ) from a M = 3 stochastic simulation.

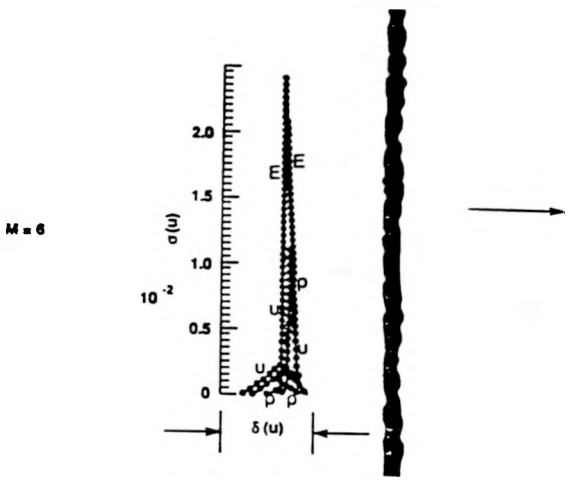

Fig. 6. Ensemble averaged pdf's of individual realizations for internal energy (E), velocity (U), and density (ρ) from a M = 6 stochastic simulation.

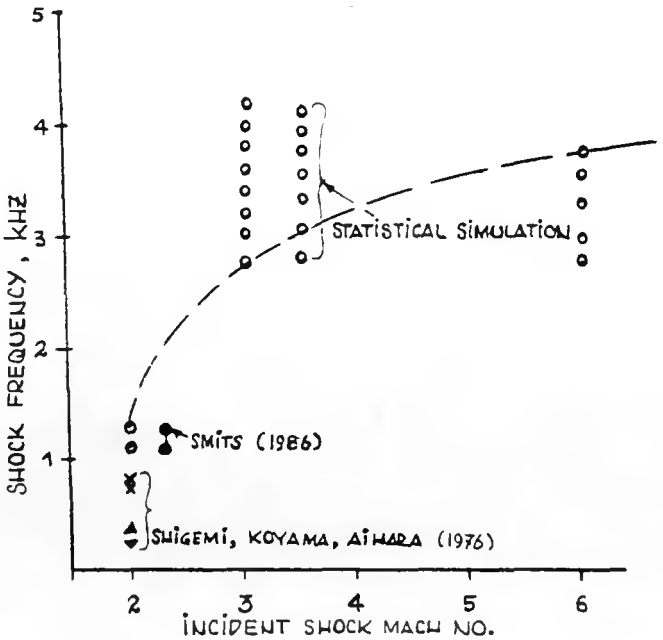

Fig. 7. Shock wave oscillating frequency as a function of shock Mach Number. Experimental resonance tube and stochastic simulation results.

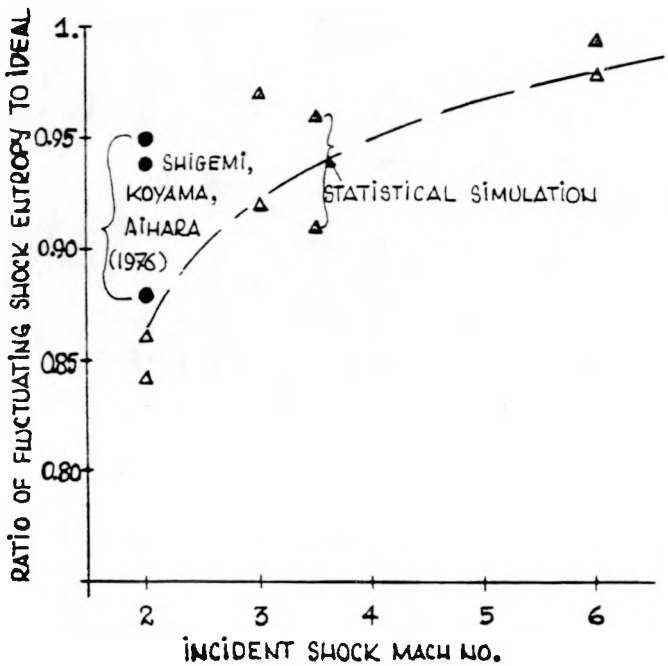

Fig. 8. Entropy change as a function of shock Mach Number for a turbulence excited shock front ratioed to that for a plane shock wave propagating in undisturbed ideal gas.

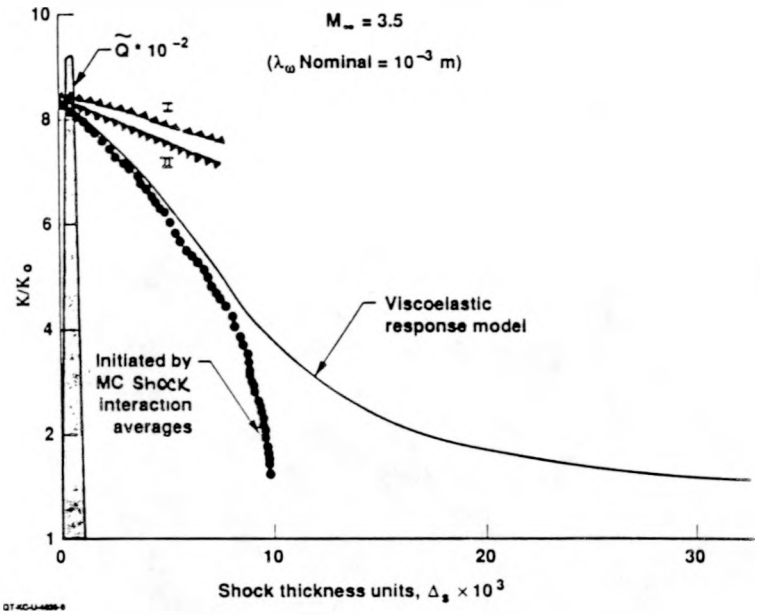

Fig. 9. Viscoelastic response implied by turbulence kinetic energy profiles vs. transitional distance through a shock wave.